



ELSEVIER

Physica D 162 (2002) 208–232

PHYSICA D

www.elsevier.com/locate/physd

Stability of β -plane Kolmogorov flow

A.J. Manfroi*, W.R. Young

Scripps Institution of Oceanography, University of California at San Diego, La Jolla, CA 92093-0213, USA

Received 30 May 2001; received in revised form 28 September 2001; accepted 20 November 2001

Communicated by U. Frisch

Abstract

We show that the geophysical β -effect strongly affects the linear stability of a sinusoidal Kolmogorov flow. If α denotes the angle between the flow direction and the planetary vorticity gradient then the critical Reynolds' number, $R_c(\alpha, \beta)$, is zero for $\beta \neq 0$, provided that $\sin 2\alpha \neq 0$. In particular, the small β limit is discontinuous: $\lim_{\beta \rightarrow 0} R_c(\alpha, \beta) = 0$, rather than the classical value $R_c(\alpha, 0) = \sqrt{2}$. Moreover, though the Kolmogorov flow is non-zonal, the most unstable modes are large-scale quasizonal flows. These results are obtained using asymptotic analysis and confirmed by numerical solution. The simulations show the saturating effects of nonlinearities. © 2002 Elsevier Science B.V. All rights reserved.

PACS: 92.10.Ei; 47.15.Fe; 47.20.Ky

Keywords: Kolmogorov flow; β -Plane; Instability; Fluid dynamics

1. Introduction

The inverse energy cascade is a distinctive characteristic of two-dimensional fluid mechanics. Because of this behavior, small-scale forcing is an effective means of generating larger-scale two-dimensional turbulence in a viscous fluid [1–3]. Sivashinsky and Yakhot [4] and Gama et al. [5] have emphasized that the inverse cascade can be regarded as an example of the large-scale instability of a set of eddies sustained against viscosity by external forcing. In this situation multiple-scale techniques can be employed to obtain an analytical characterization of the instability.

One of the simplest flows that can generate large-scale instabilities is the much-studied [4,6–9] Kolmogorov flow, whose streamfunction representation is

$$\Psi = -\Psi_0 \cos mx. \quad (1)$$

With our sign convention, the velocity is $(u, v) = (0, m\Psi_0 \sin mx)$. The Reynolds' number of the Kolmogorov flow is defined as $R \equiv \Psi_0/\nu$, where ν is the viscosity. Without complicating factors, the flow in (1) is linearly unstable to large-scale perturbations if R is greater than the critical value of $R_c = \sqrt{2}$ [8].

* Corresponding author. Tel.: +1-858-534-1504; fax: +1-858-534-8045.
E-mail addresses: amanfroi@ucsd.edu (A.J. Manfroi), wryoung@ucsd.edu (W.R. Young).

This paper is concerned with the consequences of the geophysical β -effect for the instability of the Kolmogorov flow in (1). We show that even in the limit $\beta \rightarrow 0$ the generic effect of β is to reduce the critical Reynolds' number from $\sqrt{2}$ to zero. "Generic" means that if the planetary rotation is

$$f = f_0 + \beta y \cos \alpha + \beta x \sin \alpha \quad (2)$$

then the critical Reynolds' number is zero provided that $\sin 2\alpha \neq 0$. The angle α allows for an arbitrary orientation between the ∇f and the direction of the sinusoidal shear flow in (1). Specifically, α is the angle by which ∇f is rotated clockwise from the y -axis of the coordinate system used in (1). Notice that since the 'zonal' direction is defined as the direction of constant f , in the coordinate system used in this work the x -axis does not correspond to the zonal direction unless $\alpha = 0$. In terms of the coordinate system in (2), the streamfunction of a zonal flow has the form:

$$\psi_{\text{zonal}} = \text{a function of } (x \sin \alpha + y \cos \alpha). \quad (3)$$

The linear stability of the geophysical Kolmogorov flow has been studied by previous authors. Lorenz [10] and Gill [11] considered the stability of this flow when $\alpha = 0$ in the inviscid case. In the viscous case, Frisch et al. [12,13] took $\alpha = \pi/2$, while Manfroi and Young [14] considered $\alpha = 0$. In these works asymptotic approximations based on small β and small (k, l) were used. Dolzhanskiy [15] considered the case $\alpha = 0$ when friction from an Ekman layer is present. Stuhne [16] considered the case $\alpha = 0$ in full spherical geometry. These earlier works miss the large-scale $R_c = 0$ instability which occurs provided that $\sin 2\alpha \neq 0$.

Our initial motivation for considering general α was to understand the transition between the case $\alpha = 0$ considered in [14,15] and the case $\alpha = \pi/2$ in [12,13]. The discovery of a new mode of large-scale instability with $R_c = 0$ at intermediate values of α was confusing and surprising.

In geophysical problems the choice of α depends on the physical interpretation of the small-scale Kolmogorov flow. One scenario is that the small-scale forced flow represents baroclinic disturbances, while the large-scale instability models the zonal jets which develop as a response which is secondary to baroclinic instability [17]. In other words, baroclinic instability creates disturbances whose length scale is the Rossby deformation radius and in many applications this is small-scale forcing. Via the inverse cascade, baroclinic eddies supply energy to larger-scale barotropic flows, with scales of several Rossby deformation radii, which develop into planetary-scale zonal jets [18–20]. For our purposes, the main point is that the orientation of maximally unstable baroclinic waves does not generally correspond to either $\alpha = 0$ nor to $\alpha = \pi/2$ [21]. On the other hand, most observed large-scale geophysical jets *are* zonal (e.g., the Antarctic Circumpolar Current, the atmospheric jet stream, or the banded structure of the Jovian atmosphere). Therefore, an important motivation for this work is to understand the consequences of applying small-scale forcing at an arbitrary orientation with respect to the gradient of planetary rotation, and how the large-scale response can be selectively zonal given a non-zonal small-scale forcing.

Much of this paper deals with the intricate linear stability problem resulting from the horizontal anisotropy introduced by both the sinusoidal flow in (1) and planetary vorticity gradient in (2). But we will make occasional excursions into the nonlinear regime. As an indication of the importance of α and β in the nonlinear regime, Fig. 1 shows numerical simulations of the instabilities of (1) with various values of α ; in all cases the basic state has $m = 32$ and the oscillations along the x -direction betray the underlying small-scale forcing. Panel (a) shows the case $\beta = 0$; the large-scale streamfunction is mostly disorganized. The other three panels show the effect of $\beta \neq 0$ and various values of α . In the three cases with $\beta \neq 0$ the large-scale flow is organized so that the streamlines are aligned along the lines of constant f , as in (3). In other words, the large-scale streamfunction is zonal no matter how the small-scale forcing is oriented.

The formulation of the stability problem for the Kolmogorov flow is presented in Section 2. This section also gives an overview of the main results. Detailed analysis of the stability for $\alpha = 0$, $0 < \alpha < \pi/2$, and $\alpha = \pi/2$ are presented in Sections 3–5, respectively. Section 6 presents concluding remarks.

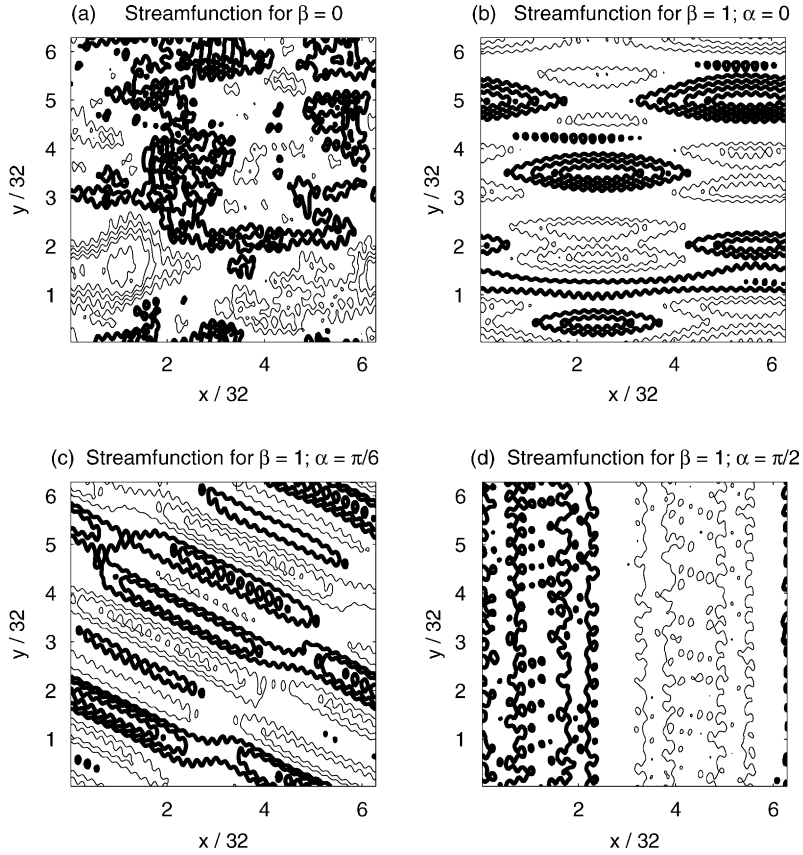


Fig. 1. Perturbation streamfunction, ψ , for four configurations of differential rotation: (a) $\beta = 0$; (b) $\beta \neq 0$ and $\alpha = 0$; (c) $\beta \neq 0$ and $\alpha = \pi/6$; (d) $\beta \neq 0$ and $\alpha = \pi/2$. The Reynolds' number is, $R = 5\sqrt{2}$ in all cases. Darker lines indicate positive values of ψ . In all three cases with $\beta \neq 0$ the large-scale flow is zonal, as in (3). The perturbation streamfunction is obtained by numerical solution of (4) with forcing at mode $(32, 0)$; the small-scale oscillations, or “wiggles”, in the x -direction are a result of this forcing. More details on the numerical method are given in Section 3.3.

2. Formulation and overview

We write the total streamfunction of a forced two-dimensional flow as $\Psi(x)$ in (1) plus a perturbation $\psi(x, y, t)$. The forcing is such that Ψ is a steady-state solution of the forced problem. One then obtains the following non-dimensionalized equation for ψ :

$$\nabla^2 \psi_t + R \sin x [\nabla^2 \psi + \psi]_y + J(\psi, \nabla^2 \psi) + \beta \cos \alpha \psi_x - \beta \sin \alpha \psi_y = \nabla^4 \psi - \mu \nabla^2 \psi, \quad (4)$$

where the Reynolds' number is $R \equiv \Psi_0/\nu$, with ν representing the viscosity. The effect of the forcing on ψ is given by the coupling with the Kolmogorov flow in the terms proportional to R . In (4), μ is a non-dimensional bottom drag, and the terms with β result from advection of the planetary vorticity in (2). The results shown in Fig. 1 are obtained by numerical solution of (4) with a resolution of 256×256 .

The stability of solutions of the linear problem associated with (4) will be the main focus of this work. The primary tool for this study is a multiple-scale analysis approach, based on β being small or R being slightly supercritical. The details of these calculations are given in Sections 3–5 and in Appendix B.

A complementary approach will be used to check and amplify the analytical results. Using a numerical eigensolver we study (4) as a Floquet problem [6,9]. This amounts to substituting

$$\psi = e^{ikx+ily+\sigma t} \sum_{n=-\infty}^{\infty} \phi_n e^{inx} \tag{5}$$

into the linearized version of (4). In (5) k and l are the wavenumbers in the x - and y -directions, respectively, and $\sigma = \sigma_r + i\sigma_i$ is the growth rate, which is a function of k, l, R, α , and β . Because one can replace k by $k + 1$ by shifting the index in the infinite sum, σ is periodic in k , with period 1. Without loss of generality then, we can confine our attention to $-\frac{1}{2} < k < \frac{1}{2}$. We also set $\mu = 0$, since in the linear problem the effect of the bottom drag is to rigidly move the spectrum in the direction of stability. Although the value of the critical Reynolds' number does depend on μ , the methods presented here can easily be extended to the case $\mu \ll 1$. Substituting (5) into (4) we obtain an eigenvalue problem, see (A.1), with eigenvalues σ . Given values of α, β and R , we define $\gamma(k, l)$ as the largest σ_r for each wavenumber (k, l) . We then define the ‘region of instability’ or ‘unstable region’ in the (k, l) -plane as the ensemble of wavenumbers for which $\gamma > 0$. The method used to numerically solve the eigenvalue problem is presented in Appendix A.

Before descending into the details of the stability analysis we now summarize the main conclusions so as to give the reader a global understanding of this stability problem. The detailed analysis supporting these results is given in Sections 3–5.

The most important result is the critical Reynolds' number, which is a function of both α and β : $R_c = R_c(\alpha, \beta)$. If $R < R_c(\alpha, \beta)$ then the flow is stable, while for $R > R_c(\alpha, \beta)$ the flow is unstable. The classical result for $\beta = 0$ [8] is

$$R_c(\alpha, 0) = \sqrt{2}. \tag{6}$$

The most surprising result in this work is that in the limit $\beta \rightarrow 0$ the critical Reynolds' number is generally not $\sqrt{2}$. In fact,

$$\lim_{\beta \rightarrow 0} R_c(\alpha, \beta) = \begin{cases} \frac{4}{5}\sqrt{2} & \text{if } \alpha = 0, \\ 0 & \text{if } 0 < \alpha < \pi/2, \\ \sqrt{2} & \text{if } \alpha = \pi/2. \end{cases} \tag{7}$$

It is important to note that the $\beta \rightarrow 0$ limit above is taken in an infinite domain. We show below that if the $\beta \rightarrow 0$ limit is taken with the domain size, L , fixed, then we recover (6).

Comparing (6) with (7), we see that there is generally a discontinuity in the value of R_c for $\beta \rightarrow 0$ and $\beta = 0$. A similar discontinuity was observed in [7], where it was shown that R_c for the flow $\Psi = \sin x + \sin \kappa y$ tends to 1 in the limit $\kappa \rightarrow 0$ and not to $\sqrt{2}$, the critical Reynolds' number for $\kappa = 0$. The conclusion in [7] was that the flows with $\kappa \neq 0$ and with $\kappa = 0$ are “absolutely different in their instability”. The same conclusion is drawn here for the flows with $\beta \neq 0$ and $\beta = 0$.

Fig. 2 shows the $\alpha = 0$ and $\pi/2$ critical curves in the (β, R) parameter plane. We present an analytic expression for $R_c(0, \beta)$ in Eq. (17). For $\alpha = \pi/2$, we can obtain an analytical expression only for small values of β : $R_c(\pi/2, \beta) = \sqrt{2} + \sqrt{6}|\beta| + O(\beta^2)$. For a generic value of β with $\alpha = \pi/2$ it is necessary to solve numerically the eigenvalue problem.

The shape of the unstable region in the (k, l) -plane depends sensitively on α . Fig. 3 shows as shaded the regions of instability with four choices of the parameters (α, β, R) . The regions of instability shown in this and the next figure are obtained from the numerical solution of the eigenproblem (A.1). Panel (a) shows the case of no differential rotation, $\beta = 0$. This is the classical case studied in [8] and the value of α is irrelevant. The value of R is slightly

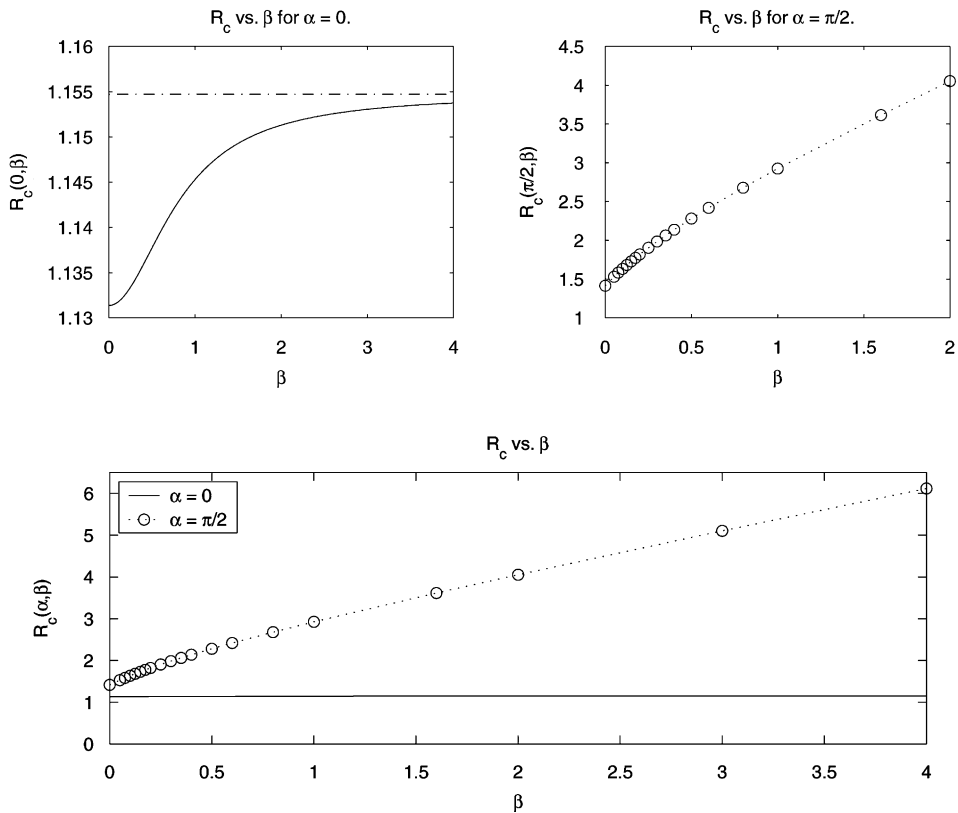


Fig. 2. Critical Reynolds' number $R_c(\alpha, \beta)$ of the Kolmogorov flow for $\alpha = 0$ and $\pi/2$. (a) $R_c(0, \beta)$ is calculated from the analytical result (17). The dot-dashed line is the asymptotic value of $\sqrt{4/3}$ obtained for $\beta \rightarrow \infty$. For $\beta \rightarrow 0$, $R_c(0, \beta) \rightarrow 4\sqrt{2}/5$. (b) For the case $\alpha = \pi/2$, $R_c(\pi/2, \beta)$ is calculated numerically by solving the eigenvalue problem. In this case as $\beta \rightarrow 0$, $R_c(\pi/2, 0) \rightarrow \sqrt{2}$. The circles indicate numerical values and the dotted line is an interpolation. (c) $R_c(0, \beta)$ and $R_c(\pi/2, \beta)$ on the same plot; notice the very small variation of $R_c(0, \beta)$.

above the critical value of $\sqrt{2}$ and the most unstable wavenumber has $k = 0$. In panel (b), $(\alpha, \beta) = (0, 0.05)$, and R is slightly above $4\sqrt{2}/5$. The crucial point is that in this case the most unstable wavenumber has $k \neq 0$ and $R_c \rightarrow 4\sqrt{2}/5 < \sqrt{2}$ for $\beta \rightarrow 0$. Panel (c) shows the case for $(\alpha, \beta) = (\pi/6, 0.05)$ and $R = 0.5$. The critical value of the Reynolds' number is zero for this case, for any $\beta > 0$. The unstable region is a sliver tangent to the line $k = l \tan \alpha$ and the most unstable wavenumber has both x and y dependence. Finally, panel (d) shows the case for $(\alpha, \beta) = (\pi/2, 0.05)$. This case is similar to the $\beta = 0$ case in panel (a) because the most unstable wavenumber has $k = 0$; the most important difference is that with $\alpha = \pi/2$ there is no instability adjacent to the origin of the (k, l) -plane.

The region of instability for $0 < \alpha < \pi/2$ is presented in Fig. 4 for various values of α . This shows the effect of varying α while keeping β and R fixed. The unstable sliver is tangent to the line $k = l \tan \alpha$ at the origin of the (k, l) -plane. Therefore, from (3), these growing disturbances are close to, but not exactly, zonal flows. We use the term “quasizonal flows”. As $\alpha \rightarrow 0$ or $\alpha \rightarrow \pi/2$ the area of the sliver reduces to zero, which is why R_c is larger than 0 for these cases.

Note that in three of the four cases in Fig. 3, the growth rate has mirror symmetry with respect to both the k -axis and the l -axis. This means that there is a quartet of unstable wavenumbers. The exception is panel (c), with $\sin 2\alpha \neq 0$,

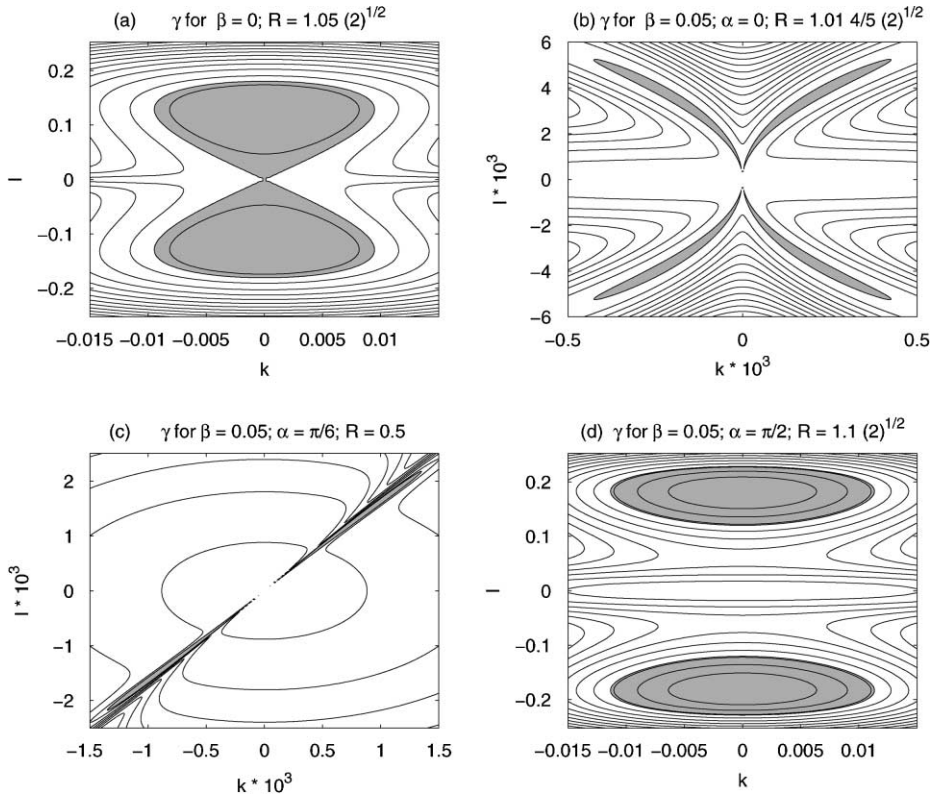


Fig. 3. Contour plots of the linear growth rate, γ , as a function of wavenumbers (k, l) for four sets of parameters. The regions of instability, where the growth rate is positive, are shaded. (a) $\beta = 0, R = 1.05\sqrt{2}$; for this case the value of α is irrelevant. (b) $\beta = 0.05, \alpha = 0$, and $R = 1.01 \times 4\sqrt{2}/5$; in this case $R_c \rightarrow 4\sqrt{2}/5$ for $\beta \rightarrow 0$. (c) $\beta = 0.05, \alpha = \pi/6$, and $R = 0.5$; for $0 < \alpha < \pi/2$ the critical Reynolds' number is 0. (d) $\beta = 0.05, \alpha = \pi/2$, and $R = 1.1\sqrt{2}$; for this case $R_c \rightarrow \sqrt{2}$ as $\beta \rightarrow 0$.

for which the growth rate is only symmetric with respect to the origin. In this case there is an unstable pair of wavenumbers. This different symmetry has a profound effect on the form of the marginally unstable disturbances. In the case $\alpha = 0$ the most unstable disturbance is a cellular pattern, like $\cos(kx) \cos(l y)$, which can be formed using four wavenumbers. But if $\sin 2\alpha \neq 0$ the most unstable disturbance is a parallel shear flow, like $\cos(kx + l y)$, which can be formed using two wavenumbers. This parallel flow is inclined at a slight angle to the zonal direction, and consequently it is really a slowing propagating Rossby wave. More details are given in Section 4.

In a finite domain, i.e. with L finite, the (k, l) wavenumbers are discretized. In both cases shown in Fig. 3(b) and (c), and in Fig. 4, the regions of instability, which have $k \neq 0$, decrease in size for $\beta \rightarrow 0$. When β is small enough none of the $k \neq 0$ discrete wavenumbers falls inside these unstable regions. Then the most unstable wavenumbers are those with $k = 0$ and (6) is recovered. In other words, because of quantization, the limits $\beta \rightarrow 0$ and $L \rightarrow \infty$ do not commute.

Thus, with α and β there are complicated changes in the Kolmogorov stability problem. A complete understanding of this problem requires analysis of the linear problem associated with (4) (using multiple-scale techniques) coupled with numerical solutions of the eigenvalue problem (A.1) (see Appendix A). As a check on these calculations we also make comparisons with numerical solutions of the full two-dimensional nonlinear equation (4). As in Fig. 1, this lets us glimpse the nonlinear saturation of the instabilities.

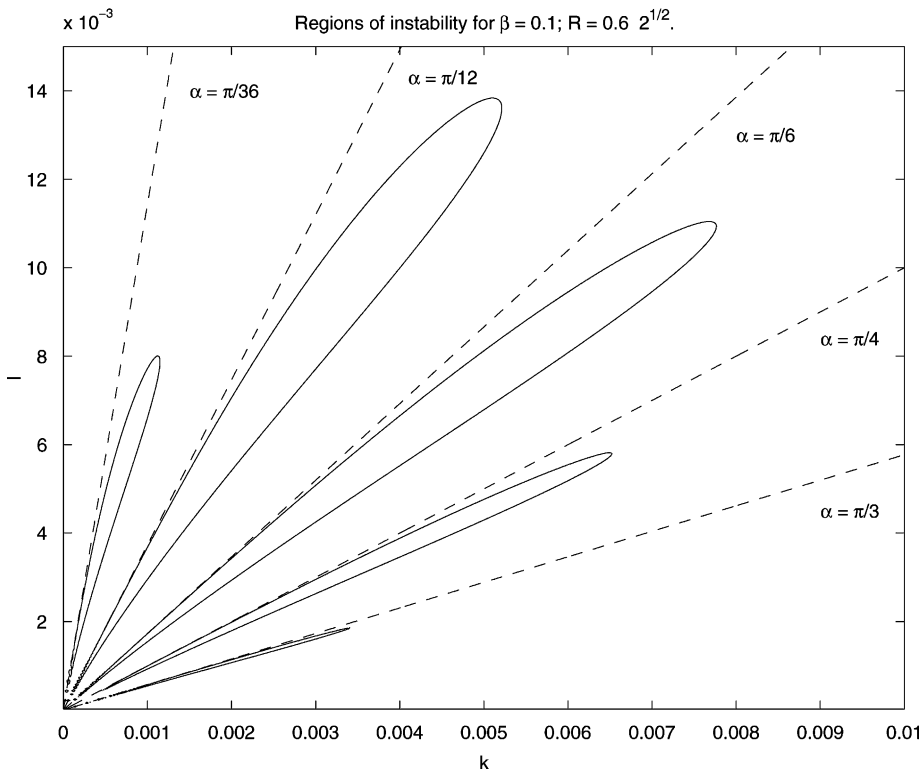


Fig. 4. Regions of instability for $\beta = 0.1$, $R = 0.6\sqrt{2}$, and different values of α . The region of instability is always tangent to the dashed lines $k = l \tan \alpha$ and vanishes as $\sin 2\alpha \rightarrow 0$.

3. Linear stability for $\alpha = 0$

We first consider the case $\alpha = 0$. In this configuration the gradient of planetary vorticity is aligned with the velocity of the Kolmogorov flow; equivalently the basic state velocity is purely meridional. Fig. 5 shows the regions of instability for $\beta = 1$ and various values of R . Because of the symmetries of γ , only the first quadrant is shown. As shown above, for $\alpha = 0$ and $\beta \neq 0$, the most unstable modes lie in a small teardrop shaped region, which protrudes from the origin of the (k, l) -plane (see Fig. 5(a)). Increasing the Reynolds' number increases the size of this teardrop. When the Reynolds' number is large enough, the modes with $k = 0$ also become unstable. So for $\beta \neq 0$ the critical Reynolds' number is less than the classical value of $\sqrt{2}$ and the most unstable modes are not the same as for $\beta = 0$. For $R \rightarrow \infty$ the region of instability expands and eventually encompasses all wavenumbers with $k^2 + l^2 < 1$.

It is also useful to plot the region of instability for a fixed value of R and different values of β , as in Fig. 6 with $R = 2\sqrt{2}$. For $\beta = 0$ the most unstable wavenumbers are for $k = 0$ and l small but finite, as shown in panel (a). When $\beta > 0$ but small, the region of instability shows a small 'bump' for small k and l , as in panel (b). This 'bump' then grows with β , while the region of unstable wavenumbers centered at $k = 0$ contracts. For large values of β , as in panels (g) and (h), the unstable region is a teardrop. In other words, β is stabilizing for the wavenumbers around $k = 0$, which are the most unstable for $\beta = 0$. But β is also destabilizing for wavenumbers in the teardrop region with $k \neq 0$. As β increases the teardrop with $k \neq 0$ becomes increasingly narrow. But there is always an unstable region in the (k, l) -plane.

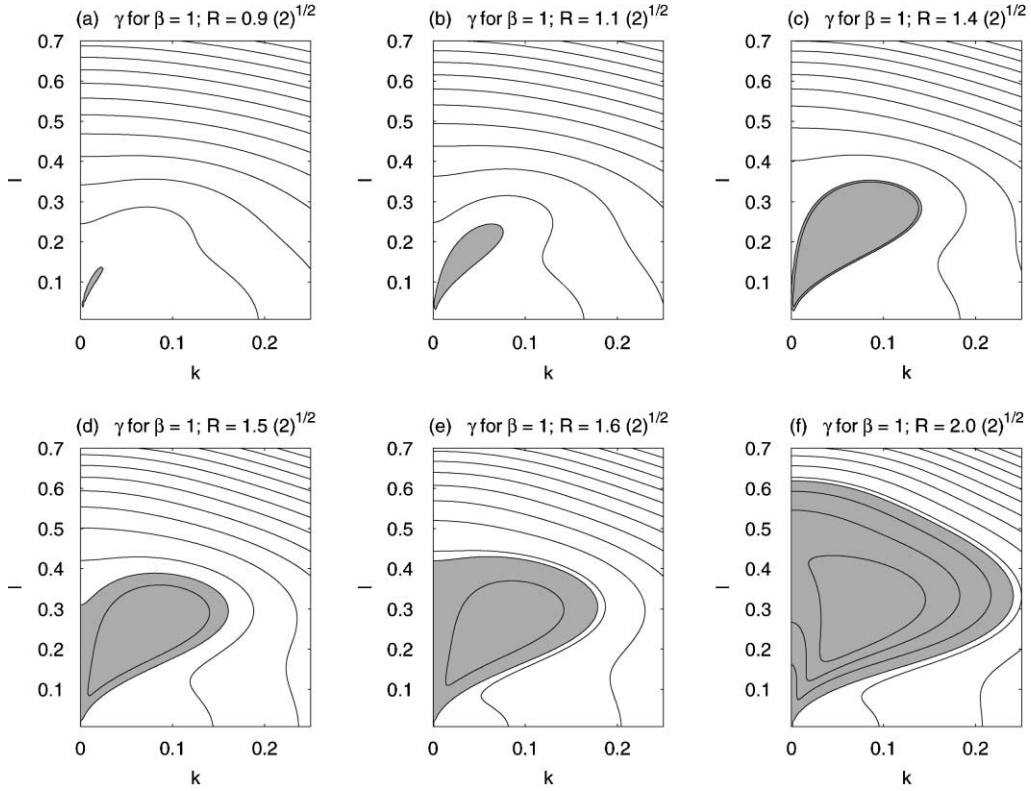


Fig. 5. Contour plots of the linear growth rate, γ , as a function of wavenumbers (k, l) for $\beta = 1$ and various values of R . For $\beta = 1$ the critical Reynolds' number is $\simeq 0.81\sqrt{2}$. The regions of instability, where the growth rate is positive, are shaded. With $\alpha = 0$ we only show the first quadrant of the (k, l) -plane, because the growth rate is symmetrical to the transformations $k \rightarrow -k$ and $l \rightarrow -l$.

3.1. Slightly supercritical Reynolds' number with $\alpha = 0$ and β unrestricted

In this section, we present some analytic results for $\alpha = 0$ obtained with multiple-scale asymptotics. We take advantage of the fact that the most unstable wavenumbers lie close to the origin of the (k, l) -plane and we use this observation to calculate $R_c(0, \beta)$. Thus, we introduce a small parameter ϵ by writing the Reynolds' number in the form $R = (1 + \epsilon^2)R_c(0, \beta)$, i.e., R is just above the critical Reynolds' number $R_c(0, \beta)$. The numerical solution of the eigenproblem motivates the multiscale expansion:

$$\partial_x \rightarrow \partial_x + \epsilon^2 \partial_\xi, \quad \partial_y \rightarrow \epsilon \partial_\eta, \quad \partial_t \rightarrow \partial_t + \epsilon^2 \partial_{t_2} + \epsilon^4 \partial_{t_4}. \tag{8}$$

The perturbation streamfunction is also expanded in orders of ϵ : $\psi = \psi_0 + \epsilon \psi_1 + \epsilon^2 \psi_2 + \dots$. With the above substitutions, one can solve the linear equation associated with (4) and the corresponding solvability condition at each order of ϵ . Here, only the main results are presented and the details are given in Appendix B.

At order $O(\epsilon^0)$ the perturbation expansion gives

$$\mathcal{L}\psi_0 = 0, \tag{9}$$

where the operator \mathcal{L} is defined as

$$\mathcal{L}\psi \equiv \psi_{xxxx} - \beta\psi_x - \psi_{txx}. \tag{10}$$

A solution of (9) is $\psi_{0x} = 0$.

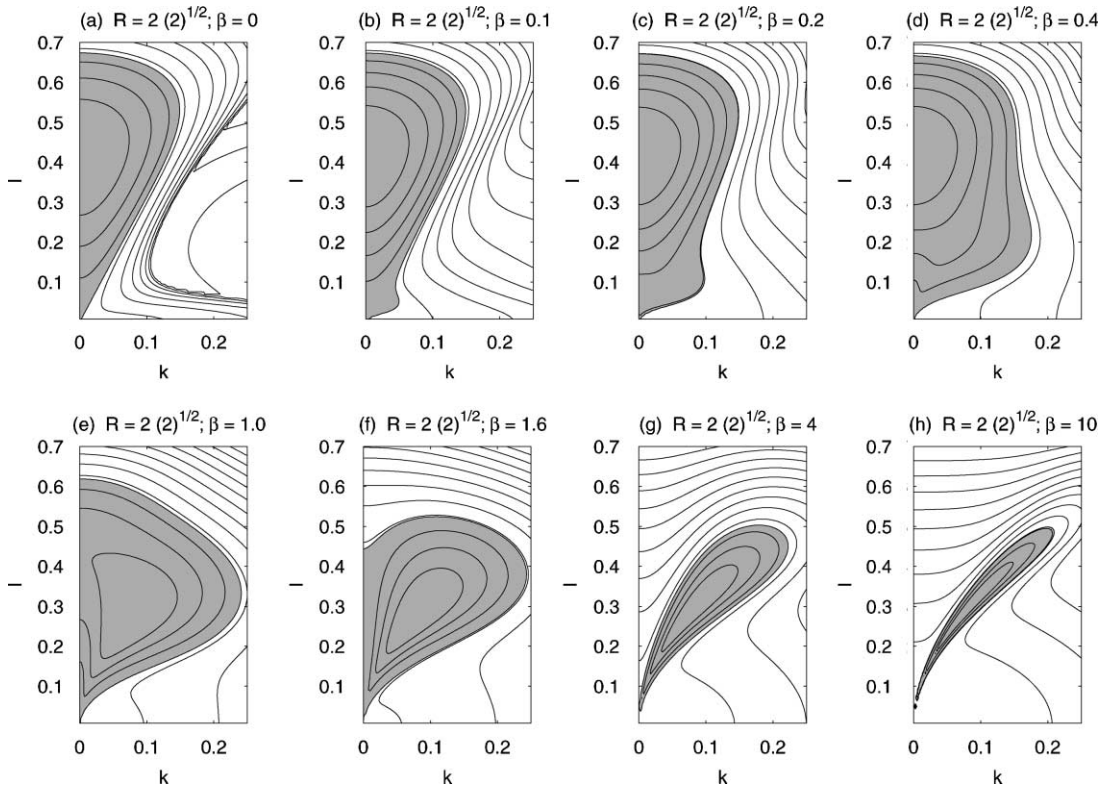


Fig. 6. Contour plots of the linear growth rate, γ , as a function of wavenumbers (k, l) for $R = 2\sqrt{2}$ and various values of β . The regions of instability, where the growth rate is positive, are shaded.

From the solvability condition at order $O(\epsilon^0)$ one has

$$\bar{\psi}_{0t\eta\eta} + \beta \bar{\psi}_{0\xi} = 0, \quad (11)$$

where an overbar indicates an average in the fast space variable x . The Rossby-like wave equation (11) can be solved with

$$\psi_0 = B(t_2, t_4)E(\xi, \eta, t) + \text{c.c.}, \quad (12)$$

where

$$E \equiv \exp(ik\xi + il\eta - i\omega t), \quad (13)$$

and the dispersion relation $\omega \equiv -\beta k/l^2$.

The first equation for the amplitude $B(t_2, t_4)$ is obtained from the order $O(\epsilon^2)$ terms of the solvability condition:

$$B_{t_2} = \sigma_2 B, \quad (14)$$

where σ_2 is a function of k, l, β , and R_c , see (B.13).

The critical Reynolds' number R_c can be obtained by setting to zero the real part of σ_2 . This gives

$$R_c^2 = 2 + 2 \frac{\omega^4 - (2\beta^2 - 3)\omega^2 + \beta^2 + \beta^4}{1 + \beta^2 + 5\omega^2}. \quad (15)$$

In this form it is evident that if $\beta = 0$ and $h \equiv k/l^2 \neq \infty$ then $R_c^2 = 2$. On the other hand, suppose we consider $\beta \neq 0$ and minimize R_c by varying $h \equiv k/l^2$. The value of h that minimizes R_c is

$$h_c^2(\beta) = \frac{-1 - \beta^2 + 2\sqrt{9\beta^4 + 13\beta^2 + 4}}{5\beta^2}. \quad (16)$$

Unpleasantly, if $\beta \rightarrow 0$, then $h_c(\beta) \rightarrow \infty$. Indeed, putting (16) into (15) one has

$$R_c^2(0, \beta) = 2 + \frac{1}{25}(8\sqrt{9\beta^4 + 13\beta^2 + 4} - 34 - 24\beta^2), \quad (17)$$

which was plotted in Fig. 2. It follows from (17) that as $\beta \rightarrow 0$, $R_c(0, \beta) \rightarrow 4\sqrt{2}/5$, and as $\beta \rightarrow \infty$, $R_c(0, \beta) \rightarrow \sqrt{4/3}$. Remarkably, $R_c(0, \beta)$ varies only by 1% over the entire range.

Having determined R_c it is now possible to obtain the amplitude equation for B at the time scale t_4 . From the $O(\epsilon^4)$ terms of the solvability condition one has

$$B_{t_4} = \sigma_4 B \quad (18)$$

with $\sigma_4(k, l, \beta, R_c)$ given in (B.17). The real part of σ_4 , denoted as γ , is the growth rate of the solution (12) at order ϵ^4 .

3.2. Small β with $\alpha = 0$ and R unrestricted

Let us now consider the confusing case of small β in more detail. Using (16) and (17) we can maximize the growth rate γ as a function of l . For small β one obtains that

$$\gamma_{\max} = \frac{5}{9}\beta^2 + O(\beta^4), \quad l_{\max}^2 = \frac{5}{9}\beta^2 + O(\beta^4), \quad (19)$$

where l_{\max} is the value of l for which γ has the maximum value γ_{\max} . Therefore, when β is small γ_{\max} is proportional to β^2 and the correct scaling for the wavenumbers (k, l) in the region of instability is $(k, l) = O(\beta)$. The scaling for k follows from $h_c = k_c/l_c^2$ being $O(\beta^{-1})$ as seen in (16).

These results suggest a different scaling in the limit of small β and unrestricted R . If one considers $\beta = \delta\beta_1$, where δ is small and positive, the suggested slow variable substitutions are

$$\partial_x \rightarrow \partial_x + \delta\partial_\xi, \quad \partial_y \rightarrow \delta\partial_\eta, \quad \partial_t \rightarrow \partial_t + \delta^2\partial_{t_2}. \quad (20)$$

Comparing (20) with (8), one important difference is that (20) uses an isotropic scaling for the space variables. One also anticipates useful results at the time scale t_2 , which is a non-trivial advantage over the previous case. Finally, in (20) the expansion parameter is really β so that without loss of generality we could set $\beta_1 = 1$. However, we prefer to retain β_1 as a flag which tags the effect of differential rotation.

The perturbation expansion can be carried out in analogy with the previous section. Only notable differences are presented here. The operator \mathcal{L} is now defined as

$$\mathcal{L}\psi \equiv \psi_{xxxx} - \psi_{txx}. \quad (21)$$

The term proportional to β is relegated to a higher order. The expansion of ψ is $\psi = \psi_0 + \delta\psi_1 + \delta^2\psi_2 + \dots$.

The solution for ψ_0 is

$$\psi_0 = B(t_2)E(\xi, \eta, t) + \text{c.c.}, \quad (22)$$

where E is still defined as in (13) but now with $\omega \equiv -\beta_1 k/(k^2 + l^2)$. The solvability condition at order $O(\delta^2)$ gives

$$B_{t_2} = \sigma_2 B, \quad (23)$$

where σ_2 is now a function of k, l, β_1 , and R .

The stability of B is determined by $\gamma \equiv \sigma_{2r}$. We find

$$\gamma \equiv -(k^2 + l^2) + l^2 R^2 \frac{l^2 - 7k^2 + 5\omega^2(k^2 + l^2)}{2(k^2 + l^2)(1 + \omega^2)^2}. \tag{24}$$

If we call R_γ the Reynolds' number for which $\gamma = 0$ then

$$R_\gamma^2 = \frac{2(k^2 + l^2)^2(1 + \omega^2)^2}{l^2[l^2 - 7k^2 + 5\omega^2(k^2 + l^2)]}. \tag{25}$$

One recovers the results of the previous section by taking the limit of $k \rightarrow 0$ with $\beta_1 k$ finite, and then minimizing R_γ with respect to k/l^2 . The result is again that $R_c = 4\sqrt{2}/5$. In other words, there is a region of overlap in which (17) and (25) are both valid.

Eq. (24) describes the growth rate for small β and unrestricted R . Fig. 7 shows a comparison of (24) with the growth rate calculated from the eigenvalue problem. The agreement is obviously better the smaller the value of β . Note also how the scaling (20) can be inferred by the scaling of the region of instability in Fig. 7 for different values of β .

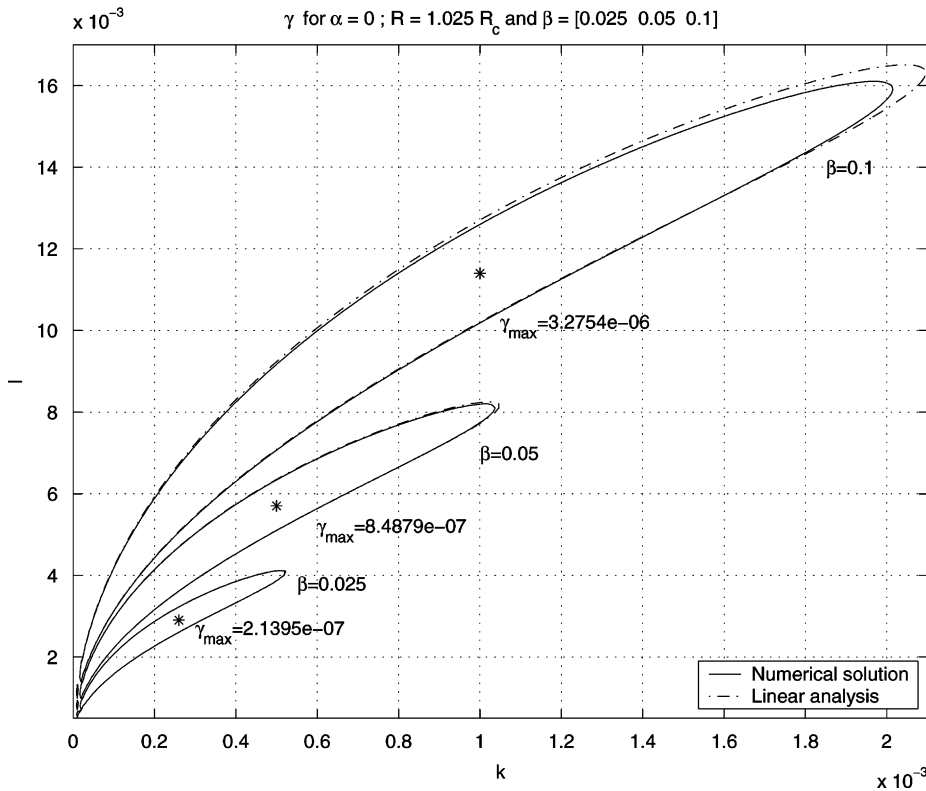


Fig. 7. Region of instability for three small values of β with $\alpha = 0$ and $R = 1.025 R_c$. The solid lines are obtained from the numerical solution of the eigenvalue problem (A.1). The dash-dotted lines are obtained from (24). The position of the wavenumber with maximum growth rate for each of the three cases is indicated by asterisks. The value of the maximum growth rate is given on the plot.

3.3. Two-dimensional nonlinear simulations and saturation of the instability for $\alpha = 0$

So far we have reached good agreement between the perturbation expansion and the numerical solution of the eigenvalue problem in the case $\alpha = 0$. The next step is to compare these results with numerical solutions of the full two-dimensional nonlinear perturbation equation (4).

We have numerically integrated (4) with periodic boundary conditions using a spectral code with a resolution of 256×256 . The nonlinear terms are calculated in real space and the code is dealiased. The domain of integration is $L \times L$ where $L = 64\pi$. In the non-dimensional notation of (4), the forcing has wavenumber $(k, l) = (1, 0)$, while the gravest wavenumber allowed in the domain of integration is $2\pi/L = 1/32$. Since we prefer to use an integer notation, we define the mode number as $32 \times (k, l)$, where (k, l) is the wavenumber. For example, the gravest mode has mode number $(1, 0)$ and the forcing is at mode number $(32, 0)$. The numerical code has enough modes to well resolve the forcing and the smaller scale nonlinear terms.

A random small-scale initial condition is used for the disturbance streamfunction ψ . There is no bottom drag, $\mu = 0$, in all the simulations presented in this paper, with the exception of a run shown in Section 6.

The first results we present are shown in Fig. 8. For this run we have chosen $\alpha = 0, \beta = 4, R = 1.25R_c$. With these parameters only one quantized mode, namely $(1, 6)$, falls inside the region of linear instability, as shown in

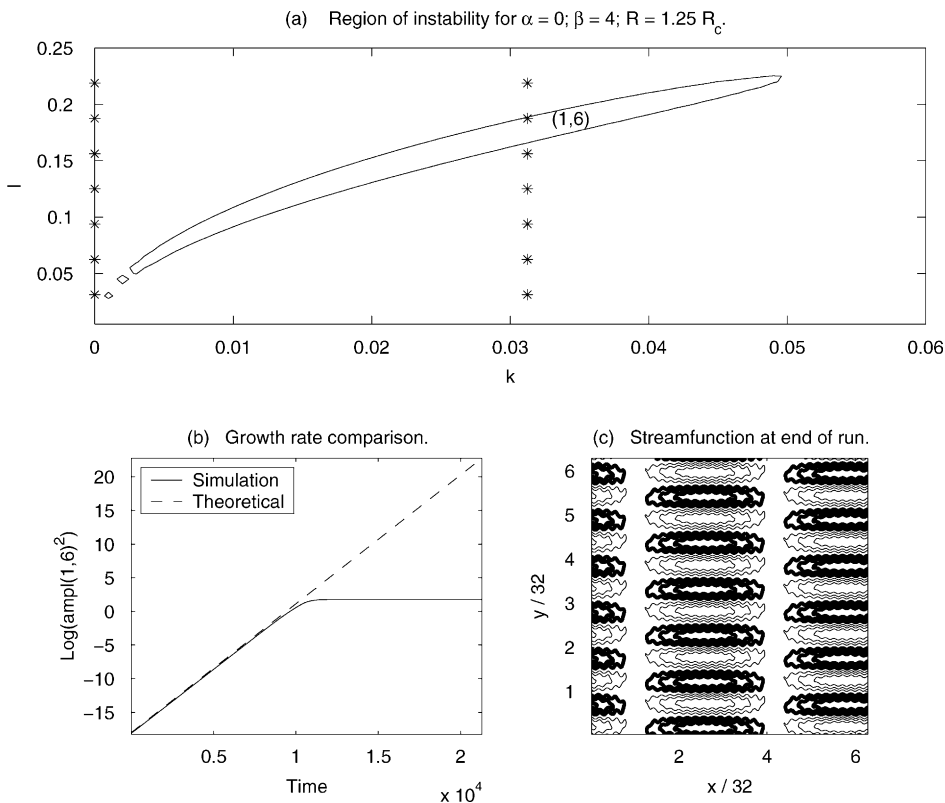


Fig. 8. Numerical simulations of the two-dimensional nonlinear perturbation equation (4) for $\alpha = 0, \beta = 4$, and $R = 1.25R_c$. (a) The region of linear instability derived from (A.1). The modes allowed by quantization are indicated by *'s. Only mode $(1, 6)$ falls inside the region of instability. (b) Growth of the amplitude of mode $(1, 6)$ from the solution of the nonlinear problem (solid curve) and from linear theory (dashed line). (c) Disturbance streamfunction, ψ , at the end of run; mode $(1, 6)$ is dominant. The small-scale oscillations are due to the forcing at mode 32.

panel (a) of Fig. 8. We therefore expect to have only mode (1, 6) grow initially, at least until nonlinearities take over. Panel (b) shows the growth of the amplitude of mode (1, 6), as a log-plot, calculated in two ways: the predicted amplitude from the growth rate for mode (1, 6) calculated from the linear eigenvalue problem (dashed line) and from the numerical integration of the nonlinear equation (4) (solid line). The agreement is gratifying for the first part of the run. Nonlinearities become important at around $t = 12\,000$, and the amplitude of the mode reaches an equilibrium. Nonlinearities have saturated the instability. The streamfunction of the perturbation ψ is shown in panel (c) at the end of the run ($t \simeq 42\,600$). The small oscillations are the effect of the forcing at mode 32. The large-scale flow is dominated by the four unstable modes ($\pm 1, \pm 6$).

4. Linear stability for $0 < \alpha < \pi/2$

We now turn to the case $0 < \alpha < \pi/2$. The most striking difference from the previous case ($\alpha = 0$) is that $R_c(\alpha, \beta) = 0$, provided only that $\sin 2\alpha \neq 0$. The shape of the region of instability is also different as seen in Fig. 9. First, notice that the growth rate $\gamma(k, l)$ has only the single symmetry $\gamma(k, l) = \gamma(-k, -l)$. Thus, it is necessary to plot $\gamma(k, l)$ in a half-plane, instead of a single quadrant.

Fig. 9(a) shows that the most unstable modes lie in a teardrop protruding from the origin of the wavenumber plane. The unstable teardrop is present even as $R \rightarrow 0$ and wavenumbers in the teardrop have $k \neq 0$. If one increases the Reynolds' number, another region of instability appears, as seen in panel (b). This second region of instability

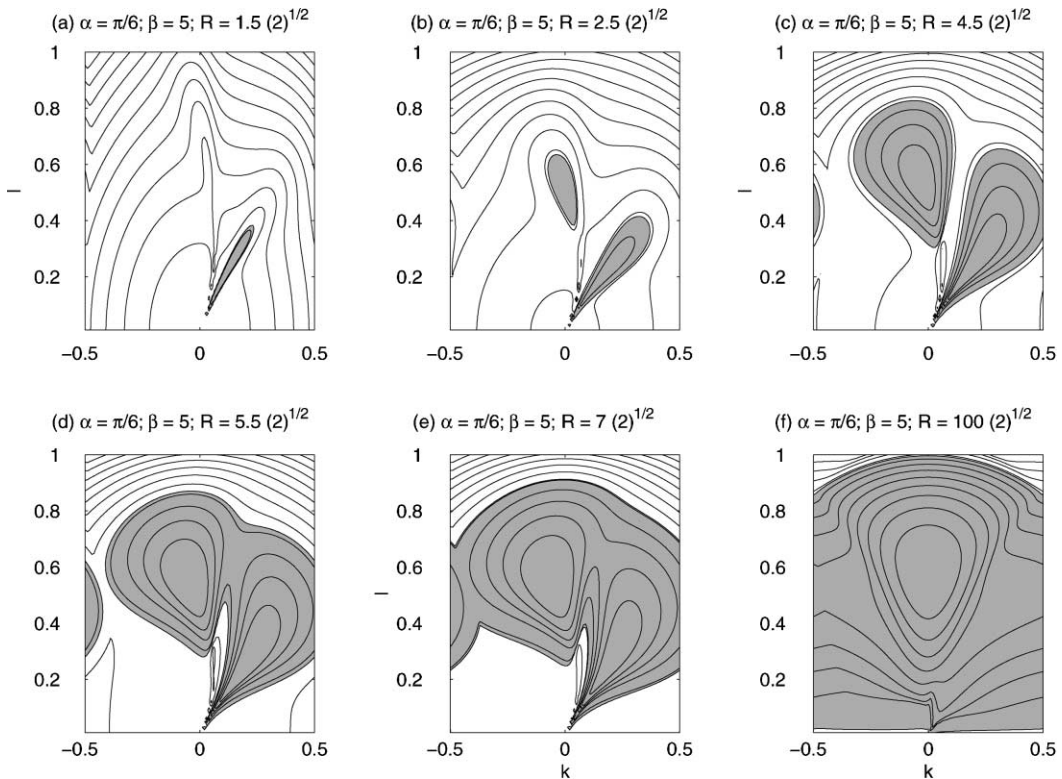


Fig. 9. Contour plots of the linear growth rate, γ , as a function of wavenumbers (k, l) for $\alpha = \pi/6$, $\beta = 5$ and various values of R . The critical Reynolds' number is 0. The regions of instability, where the growth rate is positive, are shaded.

has a higher threshold Reynolds’ number and includes the $k = 0$ wavenumbers. Increasing the Reynolds’ number further leads to the merger of these two regions of instability. When the Reynolds’ number is very large, as in panel (f), the region of instability encloses almost all wavenumbers for which $k^2 + l^2 < 1$.

4.1. Small β with $0 < \alpha < \pi/2$

To make analytical progress we confine our attention to the case of small β . In this limit the analysis can be carried over with few modifications from the analysis of Section 3.2, and our presentation will be limited to the main results.

We consider $\beta = \delta\beta_1$ and the substitutions

$$\partial_x \rightarrow \partial_x + \delta\partial_\xi, \quad \partial_y \rightarrow \delta\partial_\eta, \quad \partial_t \rightarrow \partial_t + \delta^2\partial_{t_2}. \tag{26}$$

We also define $\beta_x \equiv \beta_1 \cos \alpha$ and $\beta_y \equiv \beta_1 \sin \alpha$. The first-order perturbation ψ_0 is still given by (22) but the frequency ω is now $\omega \equiv (\beta_y l - \beta_x k)/(k^2 + l^2)$.

The solvability condition at order δ^2 gives the amplitude equation $B_{t_2} = \sigma_2 B$, and the Reynolds’ number for which the real part of σ_2 is zero is given by

$$R_\gamma^2 = \frac{2(k^2 + l^2)^2(1 + \omega^2)^2}{l^2[l^2 - 7k^2 + \omega^2(k^2 + l^2) - 4\beta_x k \omega]}, \tag{27}$$

which reduces to (25) if $\alpha = 0$.

As illustrated previously in Fig. 4, the largest unstable modes have $k = l \tan \alpha$. This suggests the introduction of a rotated coordinate system:

$$p = k \cos \alpha - l \sin \alpha, \quad q = k \sin \alpha + l \cos \alpha. \tag{28}$$

The effect of this rotation is illustrated in Fig. 10 in which the same region of instability is shown in the (k, l) and (p, q) reference frames. With (28) ω is now given by $\omega = -\beta_1 p/(p^2 + q^2)$ as expected. It is also evident from

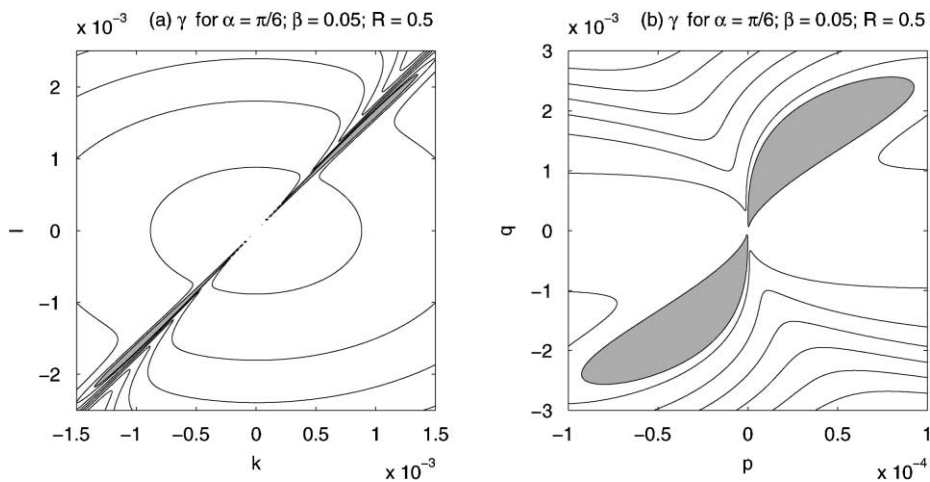


Fig. 10. Contour plots of the linear growth rate, γ , for $\beta = 0.05$, $\alpha = \pi/6$, and $R = 0.5$: (a) in the (k, l) -plane; (b) in the (p, q) -plane defined in (28). The regions of instability, where the growth rate is positive, are shaded.

Fig. 10 that the unstable wavenumbers have $p \ll q \ll 1$ and more precisely that $p \sim q^2 \ll 1$. If we use this approximation in (27), we have

$$R_\gamma^2 \simeq -\frac{q(1+\omega^2)^2}{\omega \sin 2\alpha \cos \alpha^2}, \quad (29)$$

where $\omega = O(1)$ and negative for $p > 0$. The critical Reynolds' number is given by the minimum of R_γ , which (29) shows to be zero for $q \rightarrow 0$. We conclude that $R_c = 0$ for $0 < \alpha < \pi/2$.

4.2. Two-dimensional nonlinear simulations and saturation of the instability for $0 < \alpha < \pi/2$

We turn to two-dimensional nonlinear simulations of (4) to check the results of our analysis. We consider the values $\alpha = \pi/8$, $\beta = 1$, and $R = 1$. This choice is such that there is only one quantized wavenumber in the region of instability, namely mode (1, 2), as shown in Fig. 11(a). Panel (b) shows the amplitude of mode (1, 2) as predicted by the growth rate obtained from the eigenvalue problem (A.1) (dashed line) and the results of the simulation (solid line). The agreement is again very good for the first part of the simulation. In the second part of the run, the growth of mode (1, 2) nonlinearly saturates. Panel (c) shows the streamfunction at the end of the run. The small-scale oscillations are the result of the forcing at mode (32, 0), and the large scale is dominated by mode

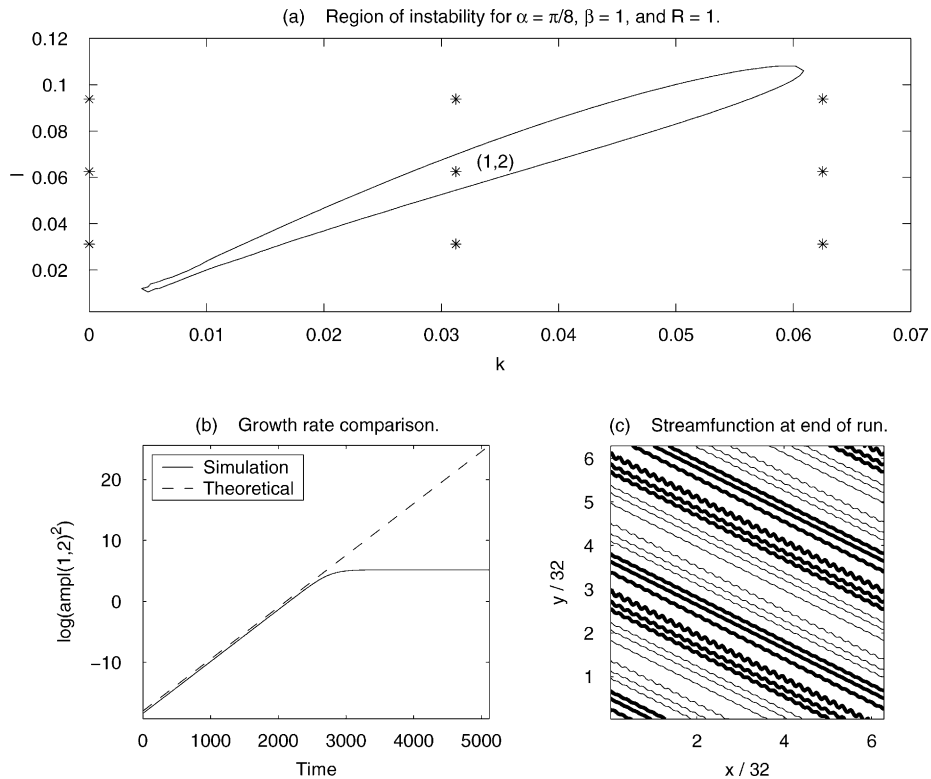


Fig. 11. Numerical simulations of the two-dimensional nonlinear perturbation equation (4) for $\alpha = \pi/8$, $\beta = 1$, and $R = 1$. (a) Region of instability obtained from the solution of the eigenproblem (A.1) and a few numerical modes (asterisks). Only mode (1, 2) falls inside the region of instability. (b) Growth of the amplitude of mode (1, 2) from the solution of the nonlinear problem (solid line) and from the eigenvalue problem (dashed line). (c) Disturbance streamfunction, ψ , at the end of run. Mode (1, 2) is the dominant large-scale mode. The small-scale oscillations are due to the forcing at mode 32.

(1, 2) as expected. Note that the streamlines in Fig. 11(c) are open while the streamlines in Fig. 8(c) have closed eddies. The difference is due to the symmetries of the system in the case $\alpha = 0$ and $0 < \alpha < \pi/2$. In the former case, all four modes $(\pm 1, \pm 6)$ are unstable. In the case presented here only modes (1, 2) and $(-1, -2)$ are unstable.

We emphasized in Section 2 that when $\sin 2\alpha \neq 0$ the most unstable disturbances are close to being zonal flows. Recall that in Fig. 4, the unstable region is tangent to the line $k = l \tan \alpha$, which implies that the disturbance streamfunction comes close to satisfying the condition for a zonal flow in (3). This point is illustrated by panel (c) of Fig. 11. The large-scale parallel flow, corresponding to mode (1, 2), makes an angle of 26.6° with the x -axis while a true zonal flow would form an angle of 22.5° . The main physical point here is that if $\sin 2\alpha \neq 0$ then large-scale instabilities are the “quasizonal flows” discussed in Section 2.

5. Linear stability for $\alpha = \pi/2$

We now turn to the case $\alpha = \pi/2$ originally studied by Frisch et al. [12]. As shown in Fig. 3, this case is intuitive in that the critical Reynolds’ number is $\sqrt{2}$ in the limit of $\beta \rightarrow 0$. Moreover, if β is not too large, the most unstable wavenumbers have $k = 0$. Nonetheless, the linear stability problem is complicated by the existence of multiple instabilities and singular limits.

Fig. 12 shows the region of instability for $\beta = 2$, $\alpha = \pi/2$ and various values of R . Using the symmetries of the growth rate we plot only the first quadrant of the (k, l) -plane. In Fig. 12(a) the Reynolds’ number

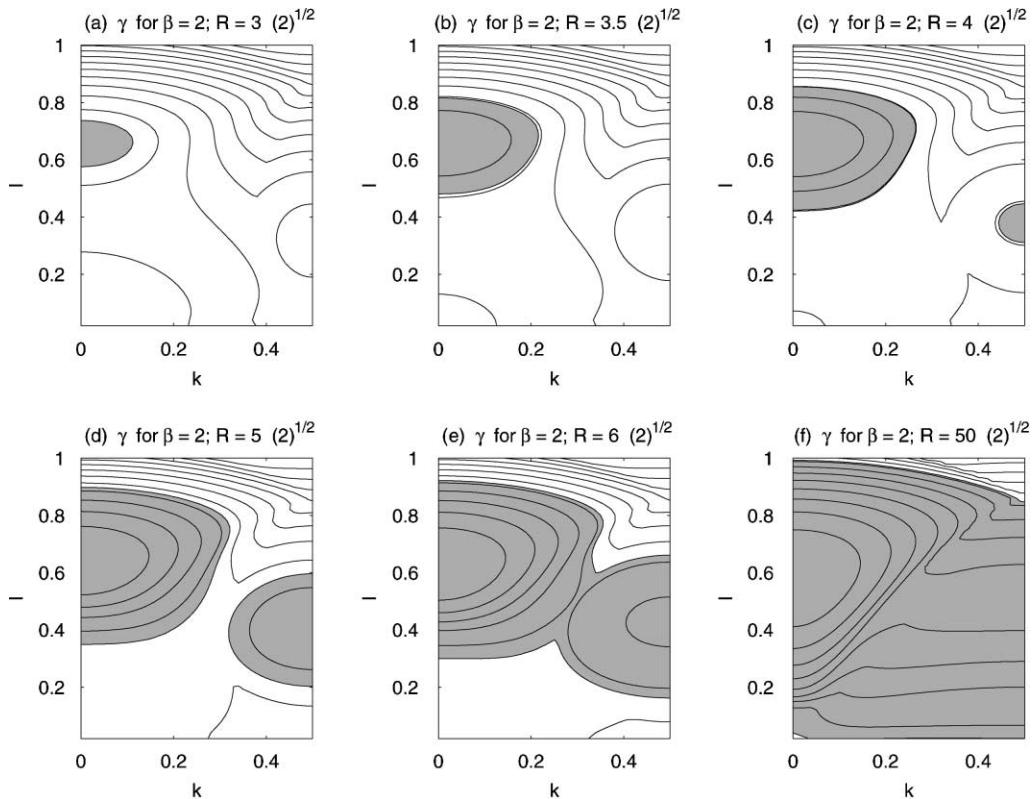


Fig. 12. Contour plots of the linear growth rate, γ , as a function of wavenumber (k, l) for $\beta = 2$, $\alpha = \pi/2$, and various values of R . For $\beta = 2$ the critical Reynolds’ number is around $2.86\sqrt{2}$. The regions of instability, where the growth rate is positive, are shaded.

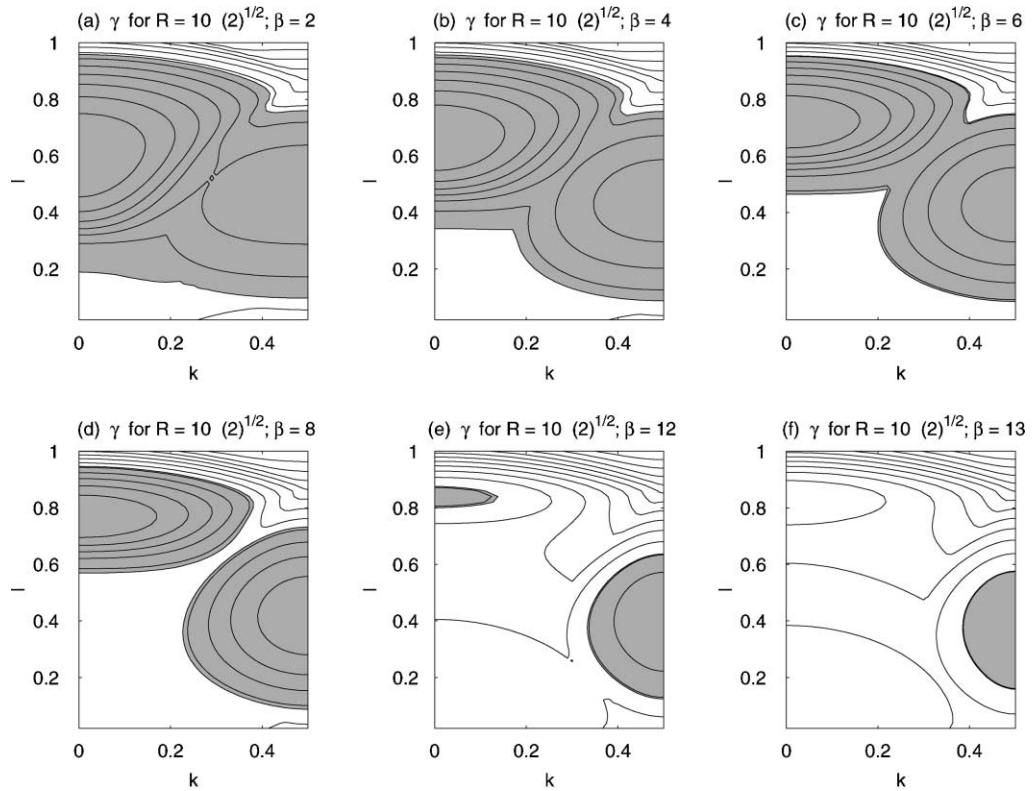


Fig. 13. Contour plots of the linear growth rate, γ , as a function of wavenumbers (k, l) for $R = 10\sqrt{2}$, $\alpha = \pi/2$ and various values of β . The regions of instability, where the growth rate is positive, are shaded.

is supercritical and there is a small region of instability centered around $k = 0$. Increasing R increases the size of the region of instability. When R is above a particular threshold value, another region of instability appears, centered at $k = 0.5$, as in panel (c). The two shaded unstable regions expand when R is increased until they merge as in panel (e). For very large values of R the region of instability occupies almost all wavenumbers with $k^2 + l^2 < 1$.

In Fig. 13 the region of instability for $R = 10\sqrt{2}$ and various values of β is shown. The unstable part of the (k, l) -plane contracts as β is increased from $\beta = 2$ as in panel (a) to $\beta = 13$ in panel (f). In panel (d) β is large enough that the two regions of instability, the one centered at $k = 0$, and the other at $k = 0.5$, become separated. Increasing the value of β further reduces the size of these regions and in panel (f) the only instability is the one centered at $k = 0.5$. Thus, for certain values of β the most unstable wavenumbers are around $k = 0.5$.

Fig. 14(a) shows the neutral curves in the (β, R) plane for the instability centered on $k = 0$ (circles) and for the second instability centered on $k = 0.5$ (triangles). If β is smaller than about 4 then the critical Reynolds' number of the $k = 0$ instability is lower than the critical Reynolds' number of the $k = 0.5$ instability. The two neutral curves intersect near $(\beta, R) = (4, 6)$ and for larger values of β the instability centered on $k = 0.5$ is the most dangerous. The curves shown in Fig. 14 have been obtained numerically, by solving repeatedly the eigenvalue problem. We cannot exclude the possibility that the stability curves may cross again for larger values of β .

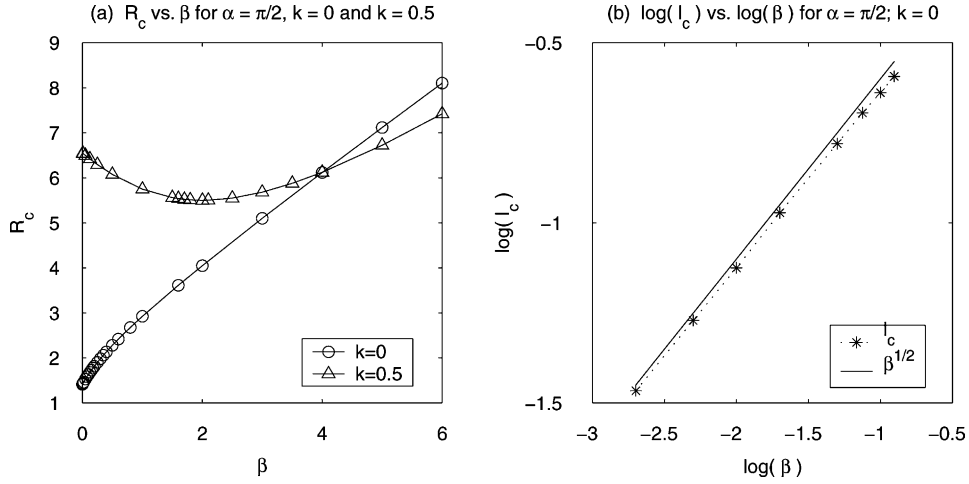


Fig. 14. (a) Critical Reynolds' number as a function of β for $\alpha = \pi/2$ and for wavenumbers with $k = 0$ (circles) and $k = 0.5$ (triangles). R_c has been obtained numerically from the eigenvalue problem (A.1) for the values of β corresponding to the circles or the triangles. The solid line connects the numerical data. (b) l_c for $\alpha = 0$ and $R = R_c$ as a function of β ($k = 0$). The asterisks are numerical data and the solid line shows the $\beta^{1/2}$ slope.

5.1. Small β and $\alpha = \pi/2$

In this section, we give an analytic expression for the neutral curve of the $k = 0$ wavenumber in the $\beta \rightarrow 0$ limit. As seen in Figs. 12 and 14(a), if β is small then the most unstable wavenumber has $k = 0$. If $R = R_c$ there is only one neutral wavenumber, which we indicate with $(0, l_c)$. All other wavenumbers have negative growth rate. Fig. 14(b) shows the value of l_c for different values of β obtained from the solution of the eigenvalue problem (asterisks). The solid line shows that for small β the most unstable wavenumber has $l \sim \beta^{1/2}$. This numerical result suggests a multiple-scale expansion with $\beta = \delta\beta_1$ and $\eta = \delta^{1/2}y$. However, it turns out that a more general result can be obtained at small β with the scaling $\eta = \delta y$. The $l \sim \beta^{1/2}$ instability is then recovered as a particular case. Thus, we consider the expansion:

$$\partial_x \rightarrow \partial_x, \quad \partial_y \rightarrow \delta\partial_\eta, \quad \partial_t \rightarrow \partial_t + \delta^2\partial_{t_2} + \delta^4\partial_{t_4} \quad (30)$$

with $\beta = \delta\beta_1$. We do not introduce a slow variable in the x -direction because we are limiting the analysis of this section to the $k = 0$ wavenumbers. The streamfunction is expanded as $\psi = \psi_0 + \delta\psi_1 + \delta^2\psi_2 + \dots$.

Given these substitutions the perturbation expansion proceeds in a similar way as for $\alpha = 0$ and $0 < \alpha < \pi/2$. We will point out the important differences. The operator \mathcal{L} is now

$$\mathcal{L}\psi = \psi_{xxxx} - \psi_{txx}, \quad (31)$$

and the leading order solution is given by

$$\psi_0 = B(t_2, t_4)E(\eta, t) + \text{c.c.}, \quad (32)$$

where $E \equiv \exp(il\eta - i\omega t)$, and $\omega \equiv \beta_1/l$.

The solvability condition at order δ^2 gives an amplitude equation for B at the t_2 time scale:

$$B_{t_2} = \sigma_2 B \quad (33)$$

with $\sigma_2 \equiv l^2(R^2/2\rho - 1)$ and $\rho \equiv 1 - i\omega$.

The amplitude equation at the t_4 time scale is obtained at order δ^4 :

$$B_{t_4} = \sigma_4 B, \tag{34}$$

where σ_4 is

$$\sigma_4 \equiv -\frac{R^2 l^4}{4\rho^3} (R^2 + 2\rho + 2\rho^2). \tag{35}$$

We can write the growth rate γ for the wavenumbers with $k = 0$ up to order δ^4 by reconstituting the expansion as $\gamma \equiv \delta^2 \gamma_2 + \delta^4 \gamma_4$, where γ_n is the real part of σ_n . By reabsorbing a factor of δ for each l , we have

$$\gamma = l^2 \left[\frac{R^2}{2(1 + \omega^2)} - 1 \right] - \frac{R^2 l^4}{4(1 + \omega^2)^3} [R^2(1 - 3\omega^2) + 4(1 + \omega^2)]. \tag{36}$$

The approximation in (36) is plotted as a dashed line in Fig. 15(a); the numerical solution of the eigenvalue problem is shown as a solid line. The agreement is very good for small values of l but starts to fail at around $l = 0.15$.

With the approximation for γ in (36) we would like to derive an analytic expression for R_c and l_c , but the algebra is too unwieldy. Instead, we resort to the approximation suggested by Fig. 14(b) and consider $l \sim \beta^{1/2}$ for β

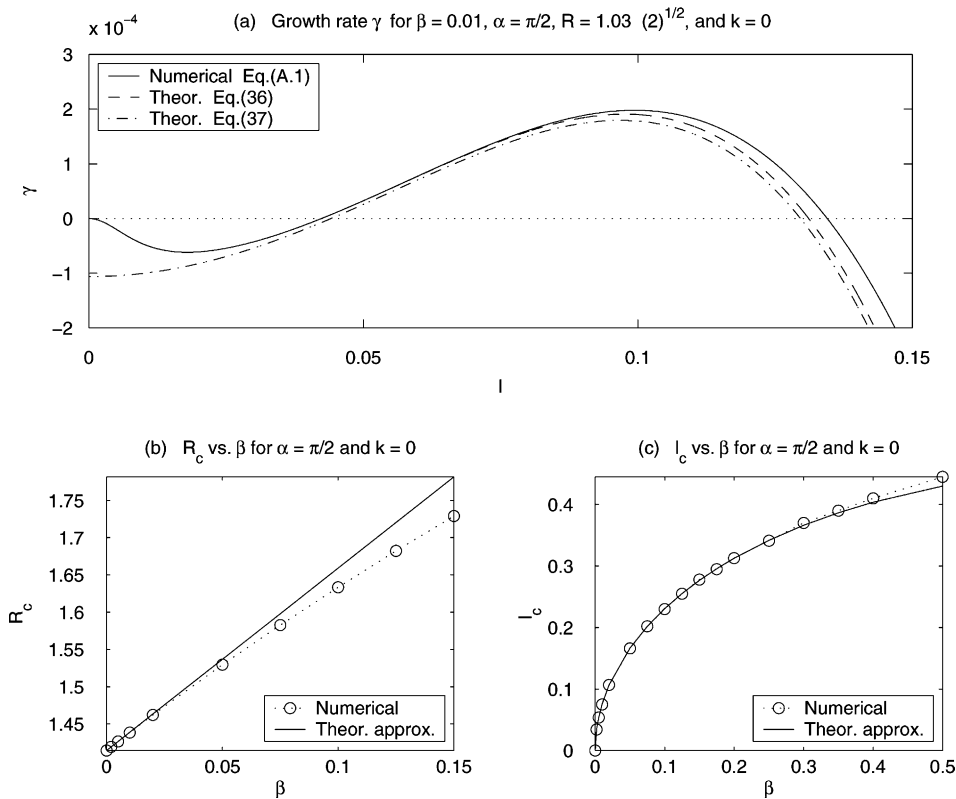


Fig. 15. (a) Comparison of the growth rate for the wavenumbers with $k = 0$ for $\beta = 0.01$ and $R = 1.03\sqrt{2}$: from the numerical solution of the eigenvalue problem (solid line), from the analytical expression in (36) (dashed line), and for the analytical approximation (37) (dash-dotted line). (b) and (c) Analytical approximations for R_c and l_c as functions of β from (37) (solid lines) compared to the numerical results (circles).

small, which also leads to $\omega \sim \beta^{1/2}$. Thus, we reduce (36) by keeping only the terms up to l^4 , or equivalently β^2 :

$$\gamma_a = -\frac{\beta^2 R^2}{2} + l^2 \left[\frac{R^2}{2} - 1 \right] - \frac{R^2 l^4}{4} [R^2 + 4]. \tag{37}$$

This simplified approximation is plotted in Fig. 15(a) as a dash-dotted line. Note that while (37) approximates the numerical solution near the most unstable wavenumber, it fails as $l \rightarrow 0$. In other words, (37) works provided l is small, but not too small. The advantage of (37) is that it is easy to calculate R_c and l_c as a series in β :

$$R_c = \sqrt{2} + \sqrt{6}|\beta| + O(\beta^2), \tag{38}$$

$$l_c = \text{sgn}(\beta)[3^{-1/4}|\beta|^{1/2} - \frac{1}{2}(3^{-3/4}|\beta|^{3/2}) + O(\beta^{5/2})]. \tag{39}$$

These approximations have been plotted in Fig. 15(b) and (c) against the numerical results. Both R_c and l_c are well approximated for small values of β .

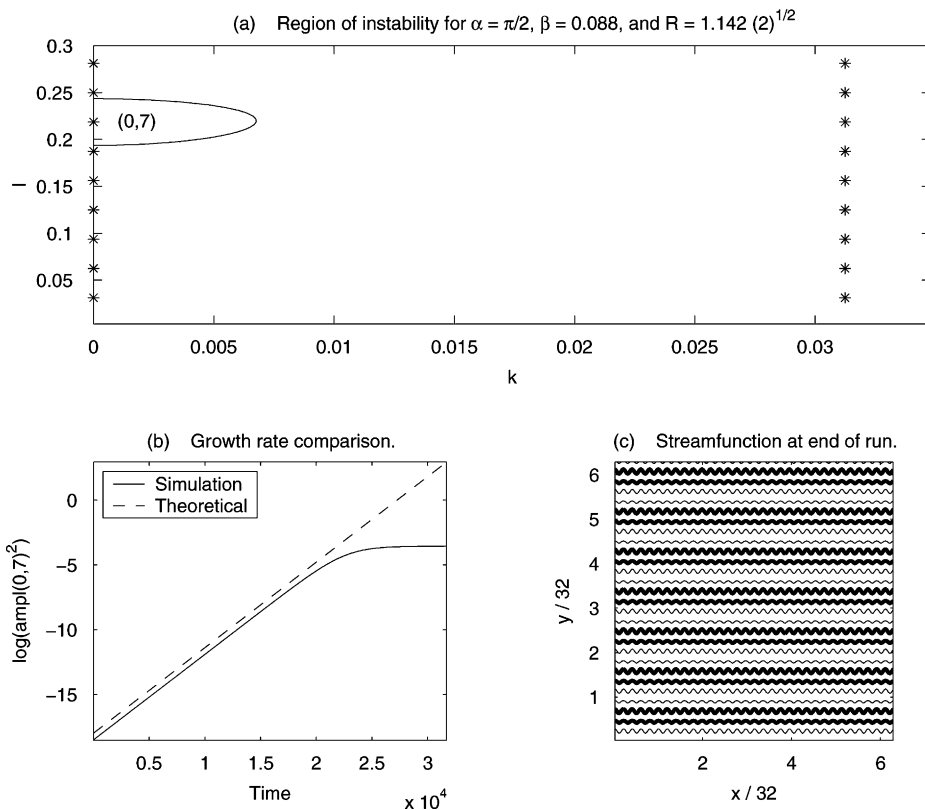


Fig. 16. Numerical simulations of the two-dimensional nonlinear perturbation equation (4) for $\alpha = \pi/2$, $\beta = 0.088$, and $R = 1.142\sqrt{2}$. (a) Region of instability derived from (A.1) and a few numerical modes (asterisks). Only mode (0, 7) falls inside the region of instability. (b) Growth of the amplitude of mode (0, 7) from the solution of the nonlinear problem (solid line) and from the eigenvalue problem (dashed line). Nonlinear saturation occur for $t > 25\,000$. (c) Disturbance streamfunction, ψ , at the end of run (the large-scale flow is meridional, not zonal). Large scales are dominated by mode (0, 7). The small-scale oscillations are due to the forcing at mode 32.

5.2. Two-dimensional nonlinear simulations and saturation of the instability for $\alpha = \pi/2$

We now turn to numerical simulations of the fully nonlinear equation (4) to test the results of the linear analysis presented above. As for the cases with $\alpha \neq \pi/2$, we choose the values for R and β so that there is only one numerical mode that is linearly unstable. We set $R = 1.142\sqrt{2}$ and $\beta = 0.088$. As Fig. 16(a) shows, for this choice only modes $(0, 7)$ and $(0, -7)$ are linearly unstable. The time evolution of the amplitude of mode $(0, 7)$ is plotted in Fig. 16(b) as derived from the numerical solution of (4) (solid line) and from the solution of the linear stability problem (dashed line). The growth of mode $(0, 7)$ is in very good agreement with the linear stability theory up to the point when nonlinearities become important (around $t = 25\,000$). Fig. 16(c) shows the disturbance streamfunction, ψ , at the end of the run. While the small scales are dominated by the forcing at mode $(32, 0)$, the large scales are dominated by mode $(0, 7)$ as predicted. Note that because $\alpha = \pi/2$ the large-scale flow in panel (c) of Fig. 16 is *meridional* (that is, the flow is perpendicular to the zonal direction).

6. Discussion and conclusions

There are two sources of anisotropy in the system that we have studied. One is the anisotropy of the instability of the Kolmogorov flow with $\beta = 0$: the most unstable mode is a flow perpendicular to the velocity of the basic state (in our notation the most unstable wavenumber has $k = 0$). The second anisotropy is due to the β -effect: as shown by Rhines [22] differential rotation tends to align streamlines in the zonal direction, along lines of constant f . In this work the angle α controls the relative orientation of these two anisotropies. For $\alpha = 0$ the two anisotropic effects reinforce each other, while for $\alpha = \pi/2$ there is maximum competition since they are orthogonal. In the latter case, the anisotropy of the flow will be determined by the relative strength of these two effects, i.e. by R and β .

This explains the stark difference between the streamfunction in Fig. 16(c) and the one in Fig. 1(d), although for both cases $\alpha = \pi/2$. In Fig. 1(d), with $R = 5\sqrt{2}$ and $\beta = 1$, the dominant anisotropic effect is given by β so that the flow is zonal. In Fig. 16(c), on the other hand, with $R = 1.142\sqrt{2}$ and $\beta = 0.088$, the flow is just slightly supercritical and β is small enough that the streamlines reflect the dominance of the slightly unstable modes $(0, 7)$ and $(0, -7)$ and not the anisotropy due to β . In this case the large-scale flow is meridional.

Our results have also important implications for the studies by Frisch et al. [12] and Manfroi and Young [14] of the weakly nonlinear problem. Both studies assumed that the effect of β on the linear stability problem was mild and this is true only if the domain is not too large.

In [12], for which $\alpha = \pi/2$, the growth rate along the $k = 0$ axis was unmodified by the effect of β . Specifically, the term $-\frac{1}{2}\beta^2 R^2$ on the right-hand side of (37) was neglected because β was assumed to be very small. Thus, even wavenumbers with $l \rightarrow 0$ were unstable. But as seen in Figs. 3 and 15(d) and (a), β stabilizes the wavenumbers with l very small. In other words, the results in [12] are valid as long as the domain is not too large, i.e. l is not too small.

In [14], for which $\alpha = 0$, it was assumed that $\lim_{\beta \rightarrow 0} R_c(\alpha, \beta) = \sqrt{2}$ and that the most unstable wavenumber has $k = 0$. Both these assumptions are valid only if none of the discrete wavenumbers with $k \neq 0$ are contained in the region of instability shown in Fig. 3(b). In this case, the most unstable discrete wavenumbers have $k = 0$ and their critical Reynolds' number is $\sqrt{2}$ for $\beta \rightarrow 0$. Again, these assumptions are justified provided that the domain is not too large.

It is worth repeating that we have neglected any effect of bottom drag in this work, i.e. we have assumed that $\mu = 0$ in (4). Indeed the effect of bottom drag on the *linear stability* is straightforward, bottom drag decreases the value of the growth rate $\gamma(k, l)$ by the constant μ . Nonetheless, if μ is large, this rigid shift of the growth rate significantly modifies the critical curve for instability, as noted in [15]. For $\mu \ll 1$, the new critical Reynolds' number for each of the cases presented in Sections 3–5 can be determined with few modifications.

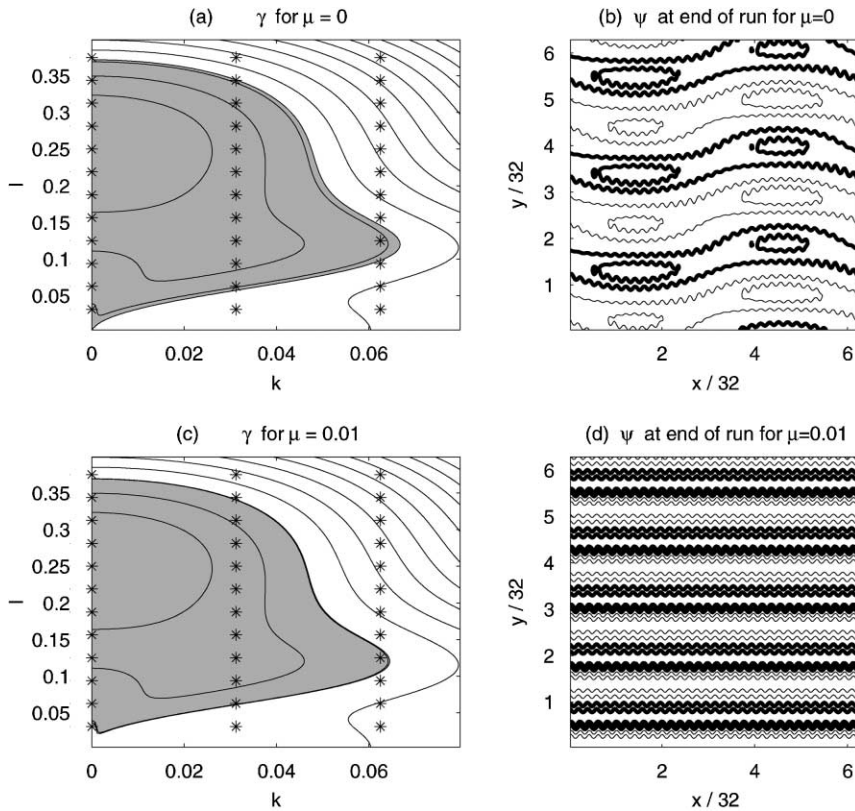


Fig. 17. Two runs with $\alpha = 0$, $\beta = 0.25$, $R = 1.25\sqrt{2}$, and $\mu = 0$ for (a) and (b), and $\mu = 0.01$ for (c) and (d). The theoretical growth rate, $\gamma(k, l)$, for $\mu = 0$ is shown in panel (a). The shaded region indicates positive growth rate. The asterisks mark the discrete modes allowed in the domain of integration. (b) The disturbance streamfunction, ψ , at $t \approx 58\,000$ from the numerical solution of (4). (c) Theoretical growth rate for $\mu = 0.01$. (d) Disturbance streamfunction, ψ , at $t \approx 58\,000$ for $\mu = 0.01$. The small-scale oscillations in (b) and (d) are due to the forcing at mode 32.

On the other hand, bottom drag has non-trivial effects on the nonlinear problem as shown by Manfroi and Young [14] and Sukoriansky et al. [23,24]. As an example we present in Fig. 17, the results of two simulations with $\alpha = 0$, $\beta = 0.25$ and $R = 1.25\sqrt{2}$, and with $\mu = 0$ and $\mu = 0.01$. Panel (a) shows the linear growth rate, $\gamma(k, l)$, for $\mu = 0$. The shaded region indicates positive growth rate. The asterisks mark the discrete modes that are allowed by the domain used in the numerical simulations. Only the discrete modes that fall into the plot have been shown: the numerical simulations have 256×256 modes. There are many modes that are linearly unstable. Panel (b) shows the disturbance streamfunction, ψ , at the end of the run ($t \approx 58\,000$). At large scales, ψ is dominated by mode (1, 3), which is one of the linearly unstable modes, although energy is present in other modes as well. Panel (c) shows the linear growth rate for $\mu = 0.01$. This small bottom drag does not significantly alter the linear growth rate: γ in panel (a) is very close to γ in panel (c). But as seen in panel (d), which shows the disturbance streamfunction for the same time ($t \approx 58\,000$) as in panel (b), ψ is dominated by mode (0, 5). Indeed, throughout the run with $\mu = 0$ the streamfunction has strong zonal dependence and ψ is dominated by modes with one zonal variation. On the other hand, there is no x -dependence in the run with $\mu = 0.01$ besides the forcing at mode 32. Thus, a small bottom drag significantly affects the nonlinear problem and has a deciding influence on the nonlinear competition among the linearly unstable modes.

Acknowledgements

We would like to thank Dr. George Carnevale and two anonymous reviewers for comments that helped to improve the manuscript. This research has been supported by the National Science Foundation under award OCE96-16017.

Appendix A. Numerical solution of the Floquet problem

To solve the eigenvalue problem obtained by substituting the Floquet type solution (5) into (4) we use the MATLAB routine “eig”. For this purpose we must limit the sum in (5) to $-N < n < N$. While we mostly use $N = 16$, we have performed several calculations with $N = 32$ to evaluate the effects of this necessary truncation. The calculations with $N = 32$ introduced changes only at the ninth significant digit to the eigenvalues. We will therefore only show results from the faster $N = 16$ calculations.

Thus, we have a matrix problem with the eigenvector $\{\phi_n\}$ and eigenvalue σ :

$$P_n^+ \phi_{n+1} + E_n \phi_n + P_n^- \phi_{n-1} = \sigma \phi_n \quad (\text{A.1})$$

with $n \in [-N, N]$ and

$$E_n \equiv i\beta \frac{\cos \alpha(n+k) - \sin \alpha l}{(n+k)^2 + l^2} - (n+k)^2 - l^2, \quad (\text{A.2})$$

$$P_n^\pm \equiv \frac{Rl}{2} \frac{(n \pm 1 + k)^2 + l^2 - 1}{(n+k)^2 + l^2}. \quad (\text{A.3})$$

The truncation is $P_N^+ = P_{-N}^- = 0$.

In general, for any given value of (k, l) , the eigenproblem (A.1) has $2N + 1$ solutions for σ , the eigenvalues. For each (k, l) we call $\tilde{\sigma}(k, l)$ the eigenvalue with the largest real part, and construct a function $\gamma(k, l)$ given by the real part of $\tilde{\sigma}(k, l)$. The function $\gamma(k, l)$ is therefore the growth rate of the most unstable mode of (4) and is a parametric function of α , β and R .

Appendix B. Linear perturbation expansion: slightly supercritical R and $\alpha = 0$

A perturbative approach can be used to study the stability of the linear problem associated with (4). Given a value of β , we consider $R = (1 + \epsilon^2)R_c$, where ϵ is a small number. As discussed in Section 3.1, we introduce slow variables and consider the following substitutions:

$$\partial_x \rightarrow \partial_x + \epsilon^2 \partial_\xi, \quad \partial_y \rightarrow \epsilon \partial_\eta, \quad \partial_t \rightarrow \partial_t + \epsilon^2 \partial_{t_2} + \epsilon^4 \partial_{t_4}. \quad (\text{B.1})$$

With these substitutions the linear problem for ψ is given by

$$\begin{aligned} & (\partial_t + \epsilon^2 \partial_{t_2} + \epsilon^4 \partial_{t_4}) [\partial_x^2 + \epsilon^2 (2\partial_x \partial_\xi + \partial_\eta^2) + \epsilon^4 \partial_\xi^2] \psi + (\epsilon + \epsilon^3) R_c \sin x [\partial_x^2 \\ & \quad + 1 + \epsilon^2 (2\partial_x \partial_\xi + \partial_\eta^2) + \epsilon^4 \partial_\xi^2] \psi_\eta + \beta \psi_x + \epsilon^2 \beta \psi_\xi \\ & = [\partial_x^4 + \epsilon^2 (4\partial_x^3 \partial_\xi + \partial_x^2 \partial_\eta^2) + \epsilon^4 (6\partial_x^2 \partial_\xi^2 + 4\partial_x \partial_\xi \partial_\eta^2 + \partial_\eta^4) + \epsilon^6 (4\partial_x \partial_\xi^3 + 2\partial_\xi^2 \partial_\eta^2) + \epsilon^8 \partial_\xi^4] \psi. \end{aligned} \quad (\text{B.2})$$

It is also useful to consider an x -average of (B.2) which gives the following solvability condition (after simplifying a factor ϵ^2):

$$\begin{aligned}
 & (\partial_t + \epsilon^2 \partial_{t_2} + \epsilon^4 \partial_{t_4})(\partial_\eta^2 + \epsilon^2 \partial_\xi^2) \bar{\psi} + (\epsilon + \epsilon^3) R_c (\overline{\sin x \psi_{\eta\eta\eta}} - 2 \overline{\cos x \psi_{\xi\eta}} + \epsilon^2 \overline{\sin x \psi_{\xi\xi\eta}}) + \beta \bar{\psi}_\xi \\
 & = \epsilon^2 \bar{\psi}_{\eta\eta\eta\eta} + 2\epsilon^4 \bar{\psi}_{\xi\xi\eta\eta} + \epsilon^6 \bar{\psi}_{\xi\xi\xi\xi},
 \end{aligned} \tag{B.3}$$

where the overbar indicates the x -average.

We then expand the perturbation streamfunction $\psi = \psi_0 + \epsilon \psi_1 + \epsilon^2 \psi_2 + \dots$ and solve (B.2) and (B.3) at each order of ϵ .

From (B.2) at $O(\epsilon^0)$ we get

$$\mathcal{L}\psi_0 = 0, \tag{B.4}$$

where the operator \mathcal{L} is defined as

$$\mathcal{L}\psi \equiv \psi_{xxxx} - \beta\psi_x - \psi_{txx}, \tag{B.5}$$

and can be solved with $\psi_{0x} = 0$.

From (B.3) at $O(\epsilon^0)$ we have

$$\bar{\psi}_{0t\eta\eta} + \beta \bar{\psi}_{0\xi} = 0, \tag{B.6}$$

which is a Rossby-like wave equation that we solve with

$$\psi_0 = B(t_2, t_4) E(\xi, \eta, t) + \text{c.c.}, \tag{B.7}$$

where

$$E \equiv \exp(ik\xi + il\eta - i\omega t), \tag{B.8}$$

and ω is given by the dispersion relation $\omega \equiv -\beta k/l^2$.

The $O(\epsilon)$ terms of (B.2) are

$$\mathcal{L}\psi_1 = R_c \sin x \psi_{0\eta}, \tag{B.9}$$

which is solved by

$$\psi_1 = s_1 B E \sin x + \text{c.c.} + c_1 B E \cos x + \text{c.c.} \tag{B.10}$$

with

$$(s_1, c_1) \equiv \frac{iR_c}{\rho^2 + \beta^2} (\rho, \beta), \tag{B.11}$$

and $\rho \equiv 1 - i\omega$.

There are no terms of $O(\epsilon)$ in (B.3).

The $O(\epsilon^2)$ terms of (B.2) give $\mathcal{L}\psi_2 = 0$ so that we can just set $\psi_2 = 0$. (Note that if we were considering also the nonlinear terms, this would not be the case and $\psi_2 \neq 0$.)

From the $O(\epsilon^2)$ terms of (B.3) we have

$$B_{t_2} = \sigma_2 B \tag{B.12}$$

with

$$\sigma_2 \equiv i\omega \frac{k^2}{l^2} + \frac{2i\beta k + l^2 \rho}{2(\rho^2 + \beta^2)} R_c^2 - l^2. \tag{B.13}$$

The terms at $O(\epsilon^3)$ of (B.2) are

$$\begin{aligned} \mathcal{L}\psi_3 = & (-2c_1k\omega - s_1\sigma_2 + i l(1 - l^2)R_c - 4ikc_1 - 2s_1l^2)BE \sin x + \text{c.c.} \\ & + (2s_1k\omega - c_1\sigma_2 + 4iks_1 - 2c_1l^2)BE \cos x + \text{c.c.}, \end{aligned} \quad (\text{B.14})$$

and we write the solution as

$$\psi_3 = s_3BE \sin x + \text{c.c.} + c_3BE \cos x + \text{c.c.} \quad (\text{B.15})$$

There are no terms of $O(\epsilon^3)$ in (B.3), and the $O(\epsilon^4)$ terms of (B.2) simply give that ψ_4 is proportional to $\sin 2x$ and $\cos 2x$.

Finally, the $O(\epsilon^4)$ terms of (B.3) give the amplitude equation

$$B_{t_4} = \sigma_4 B \quad (\text{B.16})$$

with

$$\sigma_4 \equiv -\frac{k^2}{l^2}\sigma_2 + \frac{k}{l}(c_3 + c_1)R_c - i\frac{l}{2}(s_3 + s_1)R_c - i\frac{k^2}{2l}s_1R_c - 2k^2. \quad (\text{B.17})$$

References

- [1] B. Legras, P. Santangelo, R. Benzi, High-resolution numerical experiment for forced two-dimensional turbulence, *Europhys. Lett.* 5 (1988) 37–42.
- [2] M.E. Maltrud, G.K. Vallis, Energy and enstrophy transfer in numerical simulations of two-dimensional turbulence, *Phys. Fluids A* 5 (1993) 1760–1775.
- [3] A. Chekhlov, S.A. Orszag, S. Sukoriansky, B. Galperin, I. Staroselsky, Direct numerical simulation tests of eddy viscosity in two dimensions, *Phys. Fluids* 6 (1994) 2548–2550.
- [4] G. Sivashinsky, V. Yakhot, Negative viscosity effect in large-scale flows, *Phys. Fluids* 28 (1985) 1040–1042.
- [5] S. Gama, M. Vergassola, U. Frisch, Negative eddy viscosity in isotropically forced two-dimensional flow: linear and nonlinear dynamics, *J. Fluid Mech.* 260 (1994) 95–126.
- [6] K. Gotoh, M. Yamada, Y. Mizushima, The theory of stability of spatially periodic flows, *J. Fluid Mech.* 127 (1983) 45–58.
- [7] K. Gotoh, M. Yamada, The instability of rhombic cell flows, *Fluid Dyn. Res.* 1 (1986) 165–176.
- [8] L.D. Meshalkin, I.G. Sinai, Investigation of the stability of a stationary solution of the system of equations for the plane movement of an incompressible viscous liquid, *J. Appl. Math. Mech. (Prikl. Mat. Mekh.)* 25 (1961) 1700–1705.
- [9] D.N. Beaumont, The stability of spatially periodic flows, *J. Fluid Mech.* 108 (1981) 461–474.
- [10] E.N. Lorenz, Barotropic instability of Rossby wave motion, *J. Atmos. Sci.* 29 (1972) 258–269.
- [11] A.E. Gill, The stability of planetary waves on an infinite beta-plane, *Geophys. Fluid Dyn.* 6 (1974) 29–47.
- [12] U. Frisch, B. Legras, B. Villone, Large-scale Kolmogorov flow on the beta-plane and resonant wave interactions, *Physica D* 94 (1996) 36–56.
- [13] B. Legras, B. Villone, U. Frisch, Dispersive stabilization of the inverse cascade for the Kolmogorov flow, *Phys. Rev. Lett.* 82 (1999) 4440–4443.
- [14] A.J. Manfroi, W.R. Young, Slow evolution of zonal jets on the beta plane, *J. Atmos. Sci.* 56 (1999) 784–800.
- [15] F.V. Dolzhanskiy, Effect of Ekman layer on the stability of planetary waves, *Izvestiya Atmos. Ocean Phys.* 21 (1985) 292–297.
- [16] G.R. Stuhne, One-dimensional dynamics of zonal jets on rapidly rotating spherical shells, *Physica D* 149 (2001) 43–79.
- [17] R.L. Panetta, Zonal jets in wide baroclinically unstable regions: persistence and scale selection, *J. Atmos. Sci.* 50 (1993) 2073–2106.
- [18] R. Salmon, Baroclinic instability and geostrophic turbulence, *Geophys. Astrophys. Fluid Dyn.* 15 (1980) 167–211.
- [19] A.J. Simmons, B.J. Hoskins, The life cycles of some nonlinear baroclinic waves, *J. Atmos. Sci.* 35 (1978) 414–432.
- [20] I.N. James, L.J. Gray, Concerning the effect of surface drag on the circulation of a baroclinic planetary atmosphere, *Quart. J. R. Meteorol. Soc.* 112 (1986) 1231–1250.
- [21] J. Pedlosky, *Geophysical Fluid Dynamics*, Springer, Berlin, 1987, 710+xiv pp.
- [22] P.B. Rhines, Waves and turbulence on a beta-plane, *J. Fluid Mech.* 69 (1975) 417–443.
- [23] S. Sukoriansky, B. Galperin, A. Chekhlov, Large scale drag representation in simulations of two-dimensional turbulence, *Phys. Fluids* 11 (1999) 3043–3053.
- [24] H.-P. Huang, B. Galperin, S. Sukoriansky, Anisotropic spectra in two-dimensional turbulence on the surface of a rotating sphere, *Phys. Fluids* 13 (2001) 225–240.